

Probing neutron skin and symmetry energy with relativistic isobar collisions

Hao-jie Xu^{1,*}

¹School of Science, Huzhou University, Huzhou, Zhejiang 313000, China

Abstract. In these proceedings, we present the three proposed observables to probe the neutron skin and symmetry energy with relativistic isobar collisions, namely, the isobar ratios of the produced hadron multiplicities (N_{ch}), the mean transverse momenta ($\langle p_{\perp} \rangle$), and the net charge multiplicities (ΔQ). Our findings suggest potentially significant improvement to neutron skin and symmetry energy determination over traditional low energy methods.

1 Introduction

Recently, the STAR collaboration has published the first result of the chiral magnetic effect (CME) search in isobar $^{96}_{44}\text{Ru}+^{96}_{44}\text{Ru}$ and $^{96}_{40}\text{Zr}+^{96}_{40}\text{Zr}$ collisions at nucleon-nucleon center-of-mass energy $\sqrt{s_{\text{NN}}} = 200$ GeV [1]. While no evidence is found for the CME, the experimental data show sizeable differences in multiplicity and elliptic flow between isobar collisions, indicating significant differences in their nuclear structures, such as the neutron skin thickness and nuclear deformation.

The neutron skin thickness $\Delta r_{\text{np}} \equiv \sqrt{\langle r_n^2 \rangle} - \sqrt{\langle r_p^2 \rangle}$, the root mean square difference between neutron and proton distributions, is strongly correlated to the density slope parameter of the symmetry energy. The symmetry energy and its density dependence are crucial to our understanding of the masses and drip lines of neutron-rich nuclei and the equation of state (EOS) of nuclear and neutron star matter. The Δr_{np} has traditionally been measured by low-energy electron and hadron scatterings off nuclei [2–4], and the symmetry energy slope parameters L and L_c are extracted at the nuclear saturation density ρ_0 and critical density ρ_c , respectively [3, 5–8]. Because of the inevitable uncertainties in modeling the strong interaction of the scattering processes in quantum chromodynamics (QCD) [9], large uncertainties on the L and L_c persist. The parity-violating electroweak scattering measurement on the ^{208}Pb by the Lead Radius Experiment (PREX-II), although void of QCD uncertainties, has relatively large statistical uncertainty, $\Delta r_{\text{np}} = 0.283 \pm 0.071$ fm [10, 11]. It leads to $L = 105 \pm 37$ MeV [12], at a slight tension with $L = 75 \pm 25$ MeV [13] from traditional scattering experiments.

The sensitivity of relativistic isobar collisions to neutron skin, predicted [14, 15] and confirmed by the STAR data [1], offers a new opportunity to complement low-energy measurements with completely different systematics. Specifically, the ratios between isobar collisions of the produced hadron multiplicities (N_{ch}) [16], the mean transverse momenta ($\langle p_{\perp} \rangle$) [17], and the net charge multiplicities (ΔQ) [18] are found to be sensitive to the neutron skin

*e-mail: haojiexu@zjhu.edu.cn

difference between the isobar nuclei. Measurements of those ratios can, in turn, offer an unconventional and perhaps more precise means to probe the neutron skin.

2 Symmetry energy and density functional theory

The symmetry energy encodes the energy related to neutron-proton asymmetry in the nuclear matter EOS. It is conventionally defined in the binding energy per nucleon, approximately expressed as [19] $E(\rho, \delta) = E_0(\rho) + E_{\text{sym}}(\rho)\delta^2 + \mathcal{O}(\delta^4)$, where $\rho = \rho_n + \rho_p$ is the nucleon number density and $\delta = (\rho_n - \rho_p)/\rho$ is the isospin asymmetry with ρ_p (ρ_n) denoting the proton (neutron) density. The symmetry energy can be obtained as $E_{\text{sym}}(\rho) = \left. \frac{1}{2} \frac{\partial^2 E(\rho, \delta)}{\partial \delta^2} \right|_{\delta=0}$. At a given reference density ρ_r , the $E_{\text{sym}}(\rho)$ can be expanded in $\chi_r = (\rho - \rho_r)/3\rho_r$ as $E_{\text{sym}}(\rho) = E_{\text{sym}}(\rho_r) + L(\rho_r)\chi_r + \mathcal{O}(\chi_r^2)$, where $L(\rho_r) = 3\rho_r \left. \frac{dE_{\text{sym}}(\rho)}{d\rho} \right|_{\rho=\rho_r}$ is the density slope parameter [19]. Especially, for $\rho_r = \rho_0 \approx 0.16 \text{ fm}^{-3}$ and $\rho_c = 0.11\rho_0/0.16 \approx 0.11 \text{ fm}^{-3}$, one has $L \equiv L(\rho_0)$ and $L_c \equiv L(\rho_c)$ which characterizes the density dependence of the $E_{\text{sym}}(\rho)$ around ρ_0 and ρ_c . A strong constraint $L(\rho_c) = 47.3 \pm 7.8 \text{ MeV}$ is obtained from analyzing the data on the electric dipole polarizability in ^{208}Pb [20]. Generally, it is found that the $L(\rho_c)$ displays a particularly strong positive correlation with the Δr_{np} of heavy nuclei.

We use two different nuclear energy density functionals to describe nuclear matter EOS and the properties of finite nuclei, namely, the standard Skyrme-Hartree-Fock (SHF) model (see, e.g., Ref. [21]) and the extended SHF (eSHF) model [22]. Compared to SHF, the eSHF model contains additional momentum and density-dependent two-body forces to simulate the momentum dependence of the three-body forces effectively [22]. Fitting to data using the strategy in Ref. [23], we obtain an interaction parameter set (denoted as Lc47) within eSHF by fixing $L(\rho_c) = 47.3 \text{ MeV}$ [20] with $E_{\text{sym}}(\rho_c) = 26.65 \text{ MeV}$ [24]. We also construct two more interaction parameter sets (denoted as Lc20 and Lc70) with $L(\rho_c) = 20 \text{ MeV}$ and 70 MeV , respectively, keeping the same $E_{\text{sym}}(\rho_c)$ [24], to explore the effects of the symmetry energy (and neutron skin) variations. For the SHF calculations, we use the well-known interaction set SLy4 [25, 26]. The four interaction parameter sets give similar proton rms radius r_p for ^{96}Zr and ^{96}Ru which are experimentally well constrained, but the neutron radius r_n increases with $L(\rho_c)$ and L , leading to a positive correlation between Δr_{np} and $L(\rho_c)$ (and L) as expected. Both DFT calculations predict a halo-type neutron skin thickness for ^{96}Zr , which is crucial to our understanding of non-trivial bump structures in the ratios of the multiplicity distributions and the elliptic flows in non-central isobar collisions [1, 14, 15, 27]

3 Probes in isobar collisions

3.1 Total charge multiplicity N_{ch}

The event multiplicity produced in heavy-ion collisions is sensitive to the density distributions of the colliding nuclei, and thus the L . The absolute N_{ch} values are subject to significant model dependence because particle production in heavy ion collisions is generally hard to model precisely. The shape of the N_{ch} distribution is, on the other hand, more robust. It is determined by the interaction cross-section as a function of the impact parameter (b). We use four typical, well developed, commonly used models for relativistic heavy ion collisions to simulate the particle production: the Hijing (Heavy ion jet interaction generator, v1.411) model, the AMPT (A Multi-Phase Transport, v1.26, v2.26) model with string fragmentation (v1.26) and string melting (v2.26), and the UrQMD (Ultra relativistic Quantum Molecular Dynamics, v3.4) model. Except for the input nuclear density distributions, all parameters are set to default.

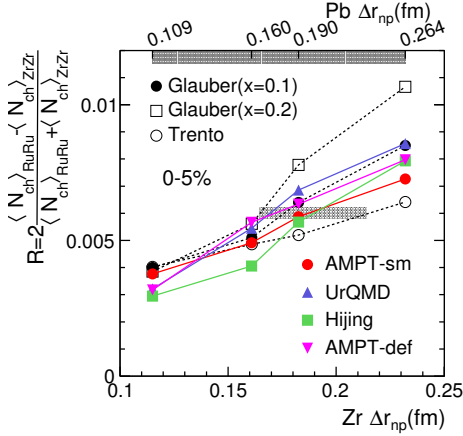


Figure 1. (Color online). The relative $\langle N_{\text{ch}} \rangle$ ratio $R_{\langle N_{\text{ch}} \rangle}$ as a function of the Zr neutron skin thickness. The four sets of data points in order from left to right are from Lc20, SLy4, Lc47, Lc70 densities. The results from AMPT-SM, UrQMD, Hijing, and AMPT-Def are connected by solid lines. The results from Glauber and Trento models are connected by dashed lines. The figure is taken from Ref. [16].

The N_{ch} distributions show splittings with different L_c . We use the relative $\langle N_{\text{ch}} \rangle$ difference between Ru+Ru and Zr+Zr, $R_{\langle N_{\text{ch}} \rangle} = 2 \frac{\langle N_{\text{ch}} \rangle_{\text{RuRu}} - \langle N_{\text{ch}} \rangle_{\text{ZrZr}}}{\langle N_{\text{ch}} \rangle_{\text{RuRu}} + \langle N_{\text{ch}} \rangle_{\text{ZrZr}}}$, to quantify the splitting of the N_{ch} tails. Experimental measurements of N_{ch} are affected by tracking inefficiency, usually multiplicity dependent [28]. While this effect mostly cancels out in $R_{\langle N_{\text{ch}} \rangle}$, it is better to use only central collisions, e.g. top 5% centrality, where the tracking efficiency is constant to a good degree.

The $R_{\langle N_{\text{ch}} \rangle}$ in each model must depend on how much the Ru and Zr nuclear density distributions differ, which can be characterized by Δr_{np} of the Zr (or Ru) nucleus. We therefore plot in Fig. 1 the $R_{\langle N_{\text{ch}} \rangle}$ in the top 5% centrality against Δr_{np} of the Zr nucleus from the eSHF (SHF) calculations with Lc20, Lc47, and Lc70 (SLy4). It is found that $R_{\langle N_{\text{ch}} \rangle}$ monotonically increases with Δr_{np} . This is because, with increasing Δr_{np} , the difference between Ru and Zr densities increases. This results in an increasing difference in N_{ch} between Ru+Ru and Zr+Zr collisions. The value of $R_{\langle N_{\text{ch}} \rangle}$ has a relatively weak model dependence, including Hijing whose tail distribution is significantly narrower than the other models, which can already be discriminated by data measurements. The intuitive geometrical models, namely, the Glauber and Trento models give a similar trend as the above dynamical models. In addition, $R_{\langle N_{\text{ch}} \rangle}$ is a relative measure between Ru+Ru and Zr+Zr collisions, and much of the experimental effects are canceled. We thus expect a precise constraint on symmetry energy with our proposed observable $R_{\langle N_{\text{ch}} \rangle}$ in relativistic isobar collisions [16].

The $R_{\langle N_{\text{ch}} \rangle}$ observable has been measured in top 2% centrality by the STAR collaboration [29]. Based on the Monte Carlo Glauber model simulations with the density distributions obtained from eSHF calculations, the symmetry energy slope parameter is extracted to be $L(\rho_c) = 53.8 \pm 1.7(\text{stat.}) \pm 7.8(\text{sys.})$ MeV, where the systematic uncertainty is dominated by those on nuclear deformations.

3.2 Mean transverse momentum $\langle p_{\perp} \rangle$

Transverse momentum (p_{\perp}) generation in relativistic heavy ion collisions is sensitive to the initial geometry and the final-state bulk evolution. In hydrodynamics, the $\langle p_{\perp} \rangle$ values are sensitive to the medium bulk properties. To investigate the effects of bulk properties, we calculate the $\langle p_{\perp} \rangle$ using the Lc47 densities with three values of shear viscosity $[(\eta/s)_{\text{min}} = 0.04, 0.08 \text{ and } 0.16]$ and with three values of bulk viscosity $[(\zeta/s)_{\text{max}} = 0.025, 0.081 \text{ and } 0.1]$ in the iEBE-VISHNU (an event-by-event (2+1)-dimensional viscous hydrodynamics, together with the hadron cascade model UrQMD) model simulations. The middle values are

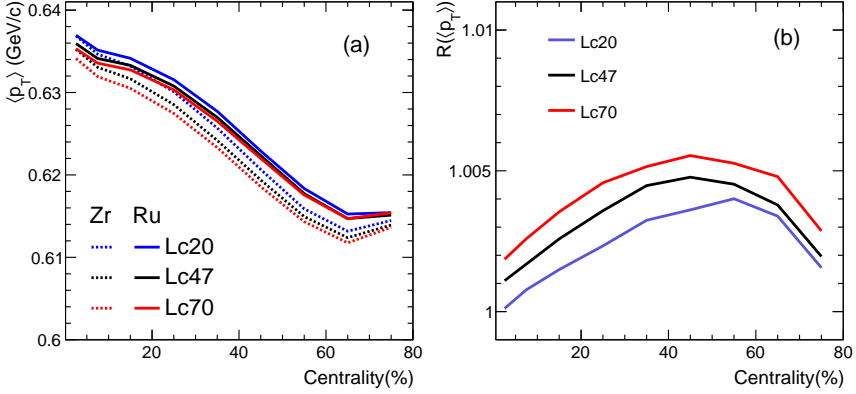


Figure 2. (Color online). (a) The mean transverse momentum $\langle p_{\perp} \rangle$ in Zr+Zr collisions, and (b) the Ru+Ru/Zr+Zr ratio $R_{\langle p_{\perp} \rangle}$ as functions of centrality, calculated by the iEBE-VISHNU model with Lc20, Lc47, and Lc70 spherical nuclear densities. Figures are taken from Ref. [17].

typical values used in hydrodynamic simulations [30]. Our findings strongly indicate while the magnitude of $\langle p_{\perp} \rangle$ depends on the bulk properties, the ratio $R_{\langle p_{\perp} \rangle} \equiv \frac{\langle p_{\perp} \rangle^{\text{Ru+Ru}}}{\langle p_{\perp} \rangle^{\text{Zr+Zr}}}$ is insensitive to them and hence their uncertainties.

Figure 2(a) presents the $\langle p_{\perp} \rangle$ as functions of centrality in both Ru+Ru and Zr+Zr collisions from the iEBE-VISHNU simulations with various DFT-calculated spherical densities for the isobars. A larger $L(\rho_c)$ gives thicker neutron skin, and results in smaller $\langle p_{\perp} \rangle$ at each centrality, as expected. On the other hand, the Ru+Ru/Zr+Zr ratio $R_{\langle p_{\perp} \rangle}$, shown in Fig. 2(b), increases with $L(\rho_c)$. This is because the neutron skin effect is larger in ^{96}Zr than in ^{96}Ru and this effect increases with $L(\rho_c)$. The splittings shown in the figure indicate the sensitivity of L_c on $R_{\langle p_{\perp} \rangle}$, providing a novel method to constrain symmetry energy in relativistic isobar collisions [17]. The centrality dependence of $R_{\langle p_{\perp} \rangle}$ is non-trivial and can reach as large as 0.5% above unity.

This method has recently been applied to the isobar data by the STAR collaboration [29]. Based on the $R_{\langle p_{\perp} \rangle}$ values in the top 5% centrality and state-of-the-art hydrodynamic simulations, the symmetry energy slope parameter has been extracted. The value is $L(\rho_c) = 56.8 \pm 0.4(\text{stat.}) \pm 10.4(\text{syst.}) \text{ MeV}$, where the systematic uncertainty is dominated by those on nuclear deformations. This result is consistent with that extracted from $R_{\langle N_{\text{ch}} \rangle}$.

3.3 Net charge ΔQ

We note that the final state N_{ch} and $\langle p_{\perp} \rangle$ do not distinguish between initial neutron or proton participants. Proton-proton (pp), proton-neutron (pn), and neutron-neutron (nn) collisions at relativistic energies produce practically the same $\langle N_{\text{ch}} \rangle$ and $\langle p_{\perp} \rangle$. It is sensitive only to the overall nucleon density, and therefore indirectly sensitive to the neutron density (and neutron skin) given that the proton density is well determined. But if nuclei had proton skin instead of neutron skin, our study would yield the same result. Ultra-peripheral collisions, where the nuclei are only grazing each other, must have very different mixture of participant protons and neutrons, and therefore likely yield significantly different net-charge numbers (ΔQ).

The ΔQ ratio in Ru+Ru over Zr+Zr collisions, under the superimposition assumption, is $R_{\Delta Q} \equiv \frac{\Delta Q_{\text{RuRu}}}{\Delta Q_{\text{ZrZr}}} = \frac{q_{\text{RuRu}} + \alpha/(1-\alpha)}{q_{\text{ZrZr}} + \alpha/(1-\alpha)}$, where $\alpha \equiv \Delta Q_{nn}/\Delta Q_{pp}$ is the ΔQ ratio in nn to pp interactions and q_{AA} is the fraction of protons among the participant nucleons that can be obtained from

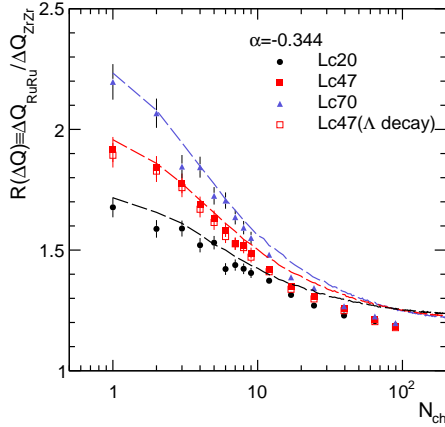


Figure 3. (Color online). $R_{\Delta Q}$ for $b \in [7, 20]$ fm as function of N_{ch} ($|\eta| < 0.5$) simulated by UrQMD with DFT nuclear densities from eSHF (Lc20, Lc47, Lc70). The open red squares show a calculation for the Lc47 case including Λ -hyperon decays. The curves are from superimposition prediction with $\alpha = -0.344$ from UrQMD NN interactions and the q_{AA} from Trento simulation. Figure is taken from Ref. [18].

Trento simulations. Pythia(version 8.240) gives $\alpha \simeq -0.352$ with acceptance cuts $|\eta| < 1$ and $0.2 < p_T < 2$ GeV/c excluding the (anti-)protons with $p_T < 0.4$ GeV/c. The overall q_{RuRu} and q_{ZrZr} values for the whole nuclei are 44/96 and 40/96, respectively; they would give $R_{\Delta Q} \simeq 1.267$. Of course, the simple superimposition assumption breaks down in non-peripheral collisions because of nuclear effects. However, the assumption should be good for grazing AA collisions. The general idea to probe Δr_{np} by $R_{\Delta Q}$ is that a sizeable Δr_{np} will make the q_{AA} decrease dramatically with increasing impact parameter (b) in those grazing collisions. The Δr_{np} of ^{96}Zr is significantly larger than that of ^{96}Ru , so the $R_{\Delta Q}$ ratio amplifies the Δr_{np} sensitivity. The Δr_{np} of both nuclei are controlled by the L_c parameter, thus a measurement of $R_{\Delta Q}$ can determine its value.

We simulate ~ 450 million events within $b \in [7, 20]$ fm using UrQMD model. The same acceptance cuts have been applied as done in Pythia simulations. Figure 3 shows $R_{\Delta Q}$ as a function of N_{ch} . Using $\alpha = -0.344$, the predicted curves from superimposition assumption are depicted in Fig. 3. The curves can fairly well describe the UrQMD data. This indicates that the grazing collisions in UrQMD, with $N_{\text{ch}} \lesssim 10$, are indeed simple superimposition of NN interactions. This is not surprising as only a few nucleons participate in such a grazing AA collision, so any nuclear effect would be negligible. At higher N_{ch} the UrQMD data points deviate from the curves, presumably because those collisions are not simple NN superimpositions anymore. It may also be viewed that the effective α in central AA collisions, because of nuclear effects, is very different from the one calculated using single NN interactions. The splittings shown in the figure indicate the sensitivity of L_c on $R_{\Delta Q}$, providing a novel method to constrain symmetry energy in relativistic isobar collisions [18].

4 Summary

The isobar $^{96}\text{Ru}+^{96}\text{Ru}$ and $^{96}\text{Zr}+^{96}\text{Zr}$ collisions at $\sqrt{s_{\text{NN}}} = 200$ GeV provide novel means to probe the neutron skins of the isobar nuclei. The neutron skin thickness can be determined, with the help of DFT calculations, from the isobar ratios of the produced hadron multiplicities ($R_{(N_{\text{ch}})}$), the mean transverse momenta ($R_{(p_{\perp})}$), and the net charge multiplicities ($R_{\Delta Q}$). Due to the rather weak dependence of these ratios to the details of QCD, our proposed methods can be used to determine the density slope parameter of symmetry energy with a precision that may be comparable to or even exceed those achieved by traditional low-energy nuclear experiments. Our measurements complement, with different systematics, those low-energy experiments in probing the symmetry energy. The preliminary results on the extracted slope

parameter $L(\rho_c)$ from $R_{(N_{ch})}$ and $R_{(p_L)}$ have been reported by the STAR collaboration [29], with the values of $53.8 \pm 1.7 \pm 7.8$ MeV and $56.8 \pm 0.4 \pm 10.4$ MeV, respectively. These values are consistent with world-wide data from traditional nuclear scattering experiments with comparable precision [29].

This work is supported by National Natural Science Foundation of China (NSFC) under Grants No. 12275082, 12035006, 12075085, 11909059.

References

- [1] M. Abdallah *et al.* [STAR], Phys. Rev. C **105**, no.1, 014901 (2022)
- [2] B. Frois and C. N. Papanicolas, Ann. Rev. Nucl. Part. Sci. **37**, 133-176 (1987)
- [3] M. B. Tsang, J. R. Stone, F. Camera *et al.*, Phys. Rev. C **86**, 015803 (2012)
- [4] C. M. Tarbert, D. P. Watts, D. I. Glazier *et al.*, Phys. Rev. Lett. **112**, 242502 (2014)
- [5] L. W. Chen, C. M. Ko and B. A. Li, Phys. Rev. C **72**, 064309 (2005)
- [6] X. Roca-Maza, M. Centelles, X. Vinas and M. Warda, Phys. Rev. Lett. **106**, 252501 (2011)
- [7] C. J. Horowitz, E. F. Brown, Y. Kim *et al.*, J. Phys. G **41**, 093001 (2014)
- [8] Y. Wang, Z. Gao, H. Lü and Q. Li, Phys. Lett. B **835**, 137508 (2022)
- [9] L. Ray, G. W. Hoffmann and W. R. Coker, Phys. Rept. **212**, 223-328 (1992)
- [10] S. Abrahamyan, Z. Ahmed, H. Albatineh *et al.*, Phys. Rev. Lett. **108**, 112502 (2012)
- [11] D. Adhikari *et al.* [PREX], Phys. Rev. Lett. **126**, 172502 (2021)
- [12] B. T. Reed, F. J. Fattoyev, C. J. Horowitz and J. Piekarewicz, Phys. Rev. Lett. **126**, 172503 (2021)
- [13] M. Centelles, X. Roca-Maza, X. Vinas and M. Warda, Phys. Rev. Lett. **102**, 122502 (2009)
- [14] H. j. Xu, X. Wang, H. Li *et al.*, Phys. Rev. Lett. **121**, 022301 (2018).
- [15] H. Li, H. j. Xu, J. Zhao *et al.*, Phys. Rev. C **98**, 054907 (2018).
- [16] H. Li, H. j. Xu, Y. Zhou *et al.*, Phys. Rev. Lett. **125**, 222301 (2020).
- [17] H. j. Xu, W. Zhao, H. Li *et al.*, [arXiv:2111.14812 [nucl-th]].
- [18] H. j. Xu, H. Li, Y. Zhou *et al.*, Phys. Rev. C **105**, L011901 (2022).
- [19] B. A. Li, L. W. Chen and C. M. Ko, Phys. Rept. **464**, 113-281 (2008)
- [20] Z. Zhang and L. W. Chen, Phys. Rev. C **90**, 064317 (2014)
- [21] E. Chabanat, J. Meyer, P. Bonche, R. Schaeffer and P. Haensel, Nucl. Phys. A **627**, 710-746 (1997)
- [22] Z. Zhang and L. W. Chen, Phys. Rev. C **94**, 064326 (2016)
- [23] Y. Zhou, L. W. Chen and Z. Zhang, Phys. Rev. D **99**, 121301 (2019)
- [24] Z. Zhang and L. W. Chen, Phys. Lett. B **726**, 234-238 (2013)
- [25] E. Chabanat, P. Bonche, P. Haensel, J. Meyer and R. Schaeffer, Nucl. Phys. A **635**, 231-256 (1998) [erratum: Nucl. Phys. A **643**, 441-441 (1998)]
- [26] X. B. Wang, J. L. Friar and A. C. Hayes, Phys. Rev. C **94**, 034314 (2016)
- [27] H. j. Xu, H. Li, X. Wang, C. Shen and F. Wang, Phys. Lett. B **819**, 136453 (2021)
- [28] B. I. Abelev *et al.* [STAR], Phys. Rev. C **79**, 034909 (2009)
- [29] H. Xu [STAR], Acta Phys. Polon. Supp. **16**, 1-A30 (2023)
- [30] J. E. Bernhard, J. S. Moreland and S. A. Bass, Nature Phys. **15**, 1113-1117 (2019)